

Optical Time-Domain Eavesdropping Risks of CRT Displays

Markus G. Kuhn

University of Cambridge, Computer Laboratory
JJ Thomson Avenue, Cambridge CB3 0FD, UK
mgk25@cl.cam.ac.uk

Abstract

A new eavesdropping technique can be used to read cathode-ray tube (CRT) displays at a distance. The intensity of the light emitted by a raster-scan screen as a function of time corresponds to the video signal convolved with the impulse response of the phosphors. Experiments with a typical personal computer color monitor show that enough high-frequency content remains in the emitted light to permit the reconstruction of readable text by deconvolving the signal received with a fast photosensor. These optical compromising emanations can be received even after diffuse reflection from a wall. Shot noise from background light is the critical performance factor. In a sufficiently dark environment and with a large enough sensor aperture, practically significant reception distances are possible. This information security risk should be considered in applications with high confidentiality requirements, especially in those that already require “TEMPEST”-shielded equipment designed to minimize radio-frequency emission-security concerns.

1. Introduction

Classic techniques for unauthorized remote access to private and confidential information – tapping communication links, code breaking, impersonation – become increasingly difficult as the use of modern cryptographic protection techniques proliferates. Those in the business of obtaining information from other people’s computers without their consent or knowledge – from law enforcement and intelligence service technicians through criminals to market researchers – are continuously looking for alternative means of access.

Military organizations have been aware of compromising acoustic and radio-frequency emanations from information processing equipment since the early 1960s and established *emission security (EMSEC)* test standards with shielding requirements for computers that process classified information [1, 2, 3]. A larger community became aware of the radio-frequency information leakage of video

displays and other computer peripherals through van Eck’s eavesdropping demonstration with modified TV sets [4] and subsequent research on related phenomena [5, 6, 7]. Optical emission security has been discussed for fiber-optic cables [8].

The available open emission-security literature on displays has so far only focused on the threat of information carried in the radio-frequency bands (primarily 3 MHz–3 GHz). We must not forget, however, that the very purpose for which display devices are designed is the emission of information suitable for human perception in the optical bands (385–790 THz frequency or 780–380 nm wavelength). As we will see, the overall light emitted by a commonly used cathode-ray tube computer monitor is a broadband information carrier that transmits via light-intensity modulation the low-pass filtered video signal. It is feasible to reconstruct screen contents from this information channel, even if the eavesdropper cannot position a sensor within a direct line-of-sight to the target display surface and receives the light only after diffuse reflection, for instance from an office wall.

An upper bound for the possible signal quality and eavesdropping distance is set by the shot noise from other light sources. Such an analysis can not only be applied to video screens but also to any other optical displays that might be targeted by an eavesdropper, for instance status indicators of serial ports.

2. Projective observation with telescopes

It has of course not escaped the attention of security experts in the past that any video display surface that is within a line of sight to an eavesdropper’s hiding place could be read with the help of a telescope. Many organizations dealing with critical information have security policies concerning the orientation and visibility of documents, computer monitors, and keyboards relative to windows that are visible from uncontrolled spaces such as nearby streets, parking lots, or buildings.

With high-quality optics, the limiting factor for the angular resolution of a telescope is the diffraction at its aperture. For an aperture (diameter of the first lens or mirror) D , the achievable angular resolution as defined by the Rayleigh criterion is

$$\theta = \frac{1.22 \cdot \lambda}{D}, \quad (1)$$

where $\lambda \approx 500$ nm is the wavelength of light. Typical modern office computer displays have a pixel size $r = 0.25$ mm (for example in the form of the 320×240 mm display area on a 43 cm CRT, divided into 1280×1024 pixels). If the observer is located at distance d and her viewing direction differs by an angle α from a perpendicular view onto the display surface, she will see a single pixel under a viewing angle $\theta = \frac{r}{d} \cdot \cos \alpha$. She will therefore need a telescope with an aperture of at least

$$D = \frac{1.22 \cdot \lambda \cdot d}{r \cdot \cos \alpha}. \quad (2)$$

A simple amateur astronomy telescope ($D = 300$ mm) will be sufficient for reading high-resolution computer display content from up to 60 m distance under $\alpha < 60^\circ$, even with very small font sizes.

3. Time-domain observation of CRT light

The direct projection of a video display surface onto the image plane of a camera with a good telescope is not the only way in which optical emanations of cathode-ray tubes can be used to read the screen content at a distance.

Most computer video displays used today are raster scan devices. As in a television receiver, the image is transmitted and updated as a sequence of scan lines that cover the entire display area with constant velocity. The pixel luminosity values in this sequence are a function of the video signal voltage. Vector displays are an alternative technique, in which not only the intensity but also the path of a cathode-ray tube electron beam is controlled by the displayed data, however they are hardly used any more.

The timing of a raster-scan video signal is first of all characterized by the pixel clock frequency f_p , which is the reciprocal of the time in which the electron beam travels from the center of one pixel to the center of its right neighbor. The pixel clock is an integer multiple of both the horizontal and vertical deflection frequency, that is the rate $f_h = f_p/x_t$ at which lines are drawn and the rate $f_v = f_p/y_t$ at which complete frames are built on the screen. Here, x_t and y_t are the total width and height of the pixel field that we would get if the electron beam needed no time to jump back to the start of the line or frame. The actually displayed image on the screen is only $x_d < x_t$ pixels wide and $y_d < y_t$ pixels high to leave time to transmit

synchronization pulses to the monitor and for the electron-beam flyback.

In order to facilitate the correct factory adjustment of the monitor image geometry over the wide range of different video timings used today, the *Video Electronics Standards Association (VESA)* has standardized a collection of exact timing parameters [9]. These include the 20–30 settings used by most personal computer displays today. An eavesdropper who has no access to the synchronization impulses from a video signal can use these standard timings as a first guess of the exact deflection frequencies. Careful additional frequency adjustment will be necessary, because the VESA timings are specified with a tolerance of 0.5%, whereas an eavesdropper has to match the correct frequency with a relative error of less than 10^{-7} to get a stable image.

The light emitted by all of the pixels of a CRT together is a weighted average of the luminosity of the last few thousand pixels that the electron beam addressed. More precisely, the intensity $I(t)$ of the light emitted is equivalent to the (gamma corrected¹) video signal $v_\gamma(t)$ convolved with the impulse response $P(t)$ of the screen phosphor:

$$I(t) = \int_0^\infty v_\gamma(t-t') P(t') dt'. \quad (3)$$

So even if an observer can pick up only the current average luminosity of a CRT surface, for example by observing with a telescope the diffuse light reflected from nearby walls, furniture, or similar objects, this provides her access to a low-pass filtered version of the video signal. Not even curtains, blinds, or windows with etched or frosted glass surfaces – as are frequently used to block views into rooms – are necessarily an effective protection, as the average luminosity inside a room can still leak out.

As with radio-frequency eavesdropping, an attacker utilizes the fact that displayed pixels are updated sequentially, and again the periodic nature of the process can be used to reduce noise and to address individual display units out of several in a room via periodic averaging.

The light emitted by a cathode-ray tube is generated when the electron beam hits a luminescent substance, called the *phosphor* (not to be confused with the chemical element phosphorous). The measurements described in the next section show that when the electron beam hits the phosphor of a bright pixel, the emitted light intensity reaches its maximum within a single pixel period, and even though the

¹The intensity of the light emitted by the phosphor is up to a saturation limit proportional to the electron beam current $i(t)$, which is typically linked to the video-signal voltage $v(t)$ by a power-law relationship $i(t) \sim (v(t) - v_0)^\gamma$. The “gamma corrected” video voltage $v_\gamma(t) \sim i(t)$ used here is strictly speaking not the actual video voltage supplied by a graphics adapter to the monitor. It is a hypothetical voltage that is proportional to the beam current and $v_\gamma(t) = 1$ V shall represent the maximum intensity. This way, we can quantify the phosphor impulse response of a monitor without having to measure the beam current.

overall afterglow of the phosphor lasts typically more than a thousand pixel times, a noticeable drop of luminosity also occurs within a single pixel time. This preserves enough high-frequency content of the video signal in the emitted light to allow for the reconstruction of readable text.

4. Characterization of phosphor decay times

The exact shape of the decay curve of the phosphors used in the CRT is an important factor for the image quality that the eavesdropper can obtain:

- It determines the frequency characteristic of the phosphor, which shows how much the high-frequency content of the video signal will be attenuated before appearing in the emitted light.
- It determines the initial luminosity during the first pixel time, which is a characteristic parameter for estimating how strong the received signal will be against the shot noise due to background light.
- It is needed as a parameter for the deconvolution operation that the eavesdropper can use to reconstruct the original image.

Every bright pixel of a CRT surface is hit by an electron beam of typically up to $100 \mu\text{A}$ for time $t_p = f_p^{-1}$, and this refresh is repeated once each time interval f_v^{-1} , where f_p and f_v are the pixel-clock and vertical-deflection frequency, respectively. The beam electrons push other electrons in the phosphor material to higher energy levels. As they fall back into their original position, they emit stored energy in the form of photons. The time delay in this process causes an afterglow for several milliseconds after the electron beam has passed by.

The user manual of the VGA CRT color monitor [10] that I used in the measurements described in the following identifies its phosphor type simply as “P22”. This is an old and obsolete designation referring to an entry in an early version of the *Electronic Industries Alliance (EIA) phosphor type registry*. It merely describes the entire class of phosphors designed for color TV applications.

The more modern *Worldwide Type Designation System (WTDS)* for CRTs [12] calls the old P22 family of phosphors “XX” instead and distinguishes subclasses. The most recent EIA TEP-116-C phosphor type registry [13] lists seven different color TV RGB phosphor type triples designated XXA (P22 sulfide/silicate/phosphate), XXB (P22 all-sulfide), XXC (P22 sulfide/vanadate), XXD (P22 sulfide/oxysulfide), XXE (P22 sulfide/oxide), XXF (P22 sulfide/oxide modified) and XXG. In addition, it contains partial information on composition, emission spectrum, decay curves and color coordinates for at least 15 further RGB

phosphor-type triplets designated XBA, XCA, etc. that were developed for data-display applications and that differ somewhat from the TV standards in their color. Unfortunately, the original manufacturer of the tested monitor has not yet been able to answer my question on which exact P22 variant was used.

CRT screen phosphors are usually based on the sulfides of zinc and cadmium or rare-earth oxysulfides and are activated by additions of dopant elements to determine the color. Most EIA registered XX and X phosphor type triplets use for the red phosphor yttrium oxysulfide doped with europium ($\text{Y}_2\text{O}_2\text{S}:\text{Eu}$), often blended with zinc phosphate doped with manganese ($\text{Zn}_3(\text{PO}_4)_2:\text{Mn}$). The green phosphor is often zinc sulfide doped with copper ($\text{ZnS}:\text{Cu}$) and sometimes also with aluminium and/or gold, or zinc silicate doped with manganese and silver ($\text{Zn}_2\text{SiO}_4:\text{Mn,Ag}$). The blue phosphor is usually zinc sulfide doped with silver ($\text{ZnS}:\text{Ag}$) and in some cases also aluminium or gallium.

Like many physical decay processes (e.g., radio activity), the luminosity of a typical excited phosphorescent substance follows an exponential law of the form

$$I_e(t) = I_0 \cdot e^{-\frac{t}{\tau}} \quad (4)$$

where I_0 is the initial luminosity right after the excitation ceases and the time constant τ is the time in which the luminosity drops by a factor e ($= 2.718$). Such decays can be identified easily in a plot of the logarithm of the luminosity over time as a straight line. For

$$\tau = \frac{1}{2\pi f} \quad (5)$$

the above exponential decay is also the impulse response of a first-order Butterworth low-pass filter consisting of a single resistor and capacitor, with a 3-dB cut-off frequency f . As the phosphor decay can be seen as a low-pass filter applied to the video signal before we can receive it with a photosensor, describing the decay in terms of the cut-off frequency is perhaps more illustrative than the time constant.

Zinc-sulfide based phosphors show instead a power-law decay curve of the form

$$I_p(t) = \frac{I_0}{(t + \alpha)^\beta} \quad (6)$$

Such a decay behavior can be identified on a plot of the logarithm of the luminosity versus the logarithm of the time since excitation has ceased as an asymptotically straight line that flattens somewhat near $t = 0$. The condition $\beta > 1$ must be fulfilled, otherwise the integral

$$\int_0^\infty \frac{1}{(t + \alpha)^\beta} dt = \frac{\alpha^{1-\beta}}{\beta - 1} \quad (7)$$

which is proportional to the total number of photons emitted would not be positive and finite.

Since commonly used phosphors are mixtures of various substances and different excitation modes occur (resulting in various wavelengths), actual decay curves have to be modeled as the sum of several exponential and power-law curves.

The TEP116-C standard provides decay curves for most phosphor types, but these are plotted on a linear time scale extending over many milliseconds. These curves give no indication about the detailed decay during the first microsecond and they are therefore not suitable for estimating the frequency characteristic of the phosphors above 1 MHz. The decay curves published in TEP116-C were measured primarily to provide information about how the phosphor type might affect the perceived flicker caused by the frame refresh. Since suitable fast decay curves or even closed form approximations were not available from the existing CRT phosphor literature, I performed my own measurements on a typical example monitor.

4.1. Instrumentation

We are primarily interested in the rapid decay within a time interval not much longer than t_p , therefore we need a very sensitive light sensor with, ideally, more than 100 MHz bandwidth or less than 5 ns rise and fall time.

One fast light sensor is the PIN photodiode in photoconductive mode, in which a reverse bias voltage is applied and the resulting current is measured. The PIN photodiode has an undoped “intrinsic” layer between the p- and n-doped regions (hence the name). Compared with normal photodiodes, PIN diodes have reduced capacity and can be used with a higher bias voltage, which increases their response time. For example, a PIN diode with a “rise and fall time of about 20 μ s” was used in [14] to evaluate the luminance decay of the P31 phosphor in a CRT used in vision research.

Photodiodes are now available with down to 1 ns response time for applications such as optical Gbit/s communication links and laser range finding. However their low sensitivity of typically 0.5 A/W makes significant additional amplification necessary, which would lead to additional noise and further limit the bandwidth. Avalanche photodiodes (APDs) provide greater sensitivity (10^2 A/W) and are also available with 1 ns response times.

Photomultiplier tubes (PMTs) are evacuated electron tubes with a photocathode. Received photons can trigger the emission of electrons, which are then accelerated with high voltage and multiplied in a cascade of further electrodes. A single received photon results in an entire cloud of electrons hitting the anode, contributing to the measured current. Photomultiplier tubes have response times in the nanosecond range and their sensitivity can be adjusted easily over many orders of magnitude.

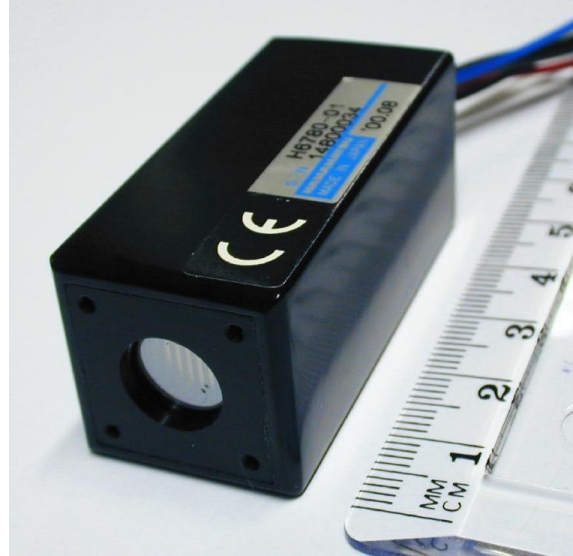


Figure 1. Photomultiplier tube module.

I used a Hamamatsu H6780-01 photosensor module (Fig. 1), which can be operated with radiant sensitivity levels in the 10^1 – 10^5 A/W range [15]. It can therefore be used under a quite wide range of light conditions. This device consists of a small robust metal package containing a photomultiplier tube and a high-voltage generating circuit. It can be operated conveniently from a 12 V lab power supply. A separately applied 0.25–0.90 V control voltage U_c adjusts the radiant sensitivity of the sensor to

$$1.5 \times 10^5 \text{ A/W} \cdot \left(\frac{U_c}{1 \text{ V}} \right)^{7.2}.$$

The radiant sensitivity is the quotient of the output current generated by the sensor and the radiant energy received by the sensor on its aperture (8 mm diameter). When operated within the specified parameters, a photomultiplier is a highly linear light-controlled current source. To prevent damage to the sensor, care must be taken to ensure that the maximum allowed average output current of 100 μ A is not exceeded, by selecting the control voltage appropriately.

According to the data sheet, the anode-current rise time of the H6780 photomultiplier module is 0.78 ns, an order of magnitude faster than the pixel time t_p of commonly used video modes. Its high sensitivity allowed me to connect it directly to the 50 Ω input of a digital storage oscilloscope with a resolution of 40 μ V.

4.2. Measurement method

In order to characterize phosphor response times, I used several test video signals that showed either a single pixel or a 320-pixel-long horizontal line, each in full intensity red,

green, blue, or white on a black background. Using both short and long pulses provides the data necessary to characterize very fast (tens of nanoseconds) as well as much slower (millisecond) features. The signal timing used was the VESA 640×480@85Hz video mode, in which the electron beam traverses a 320 mm wide screen with 18 km/s.

The decay curves of zinc-sulfide based phosphors can vary significantly under different drive conditions [16]. The EIA standard for the characterization of CRT phosphor decay times [11] therefore requires for measurements a fixed beam current of 100 μA . Lacking the equipment to measure such a current directly at the high-voltage anode connection, I simply used a default setting of monitor controls (100% contrast, 50% brightness, color temperature 6500 K, monitor powered up for at least 30 min) and the full intensity color combinations that are most frequently used for text display. The resulting luminosity measurement is therefore with respect to a known video signal voltage, not a beam current.

Placed 0.25 m in front of the center of the screen surface with an aperture of 50 mm², the photosensor, as seen from a pixel, covered a solid angle of around 0.8 msr. The oscilloscope that recorded the photosensor signal was triggered from the vertical sync signal on pin 12 of the feature connector of the driving VGA card. It recorded with 8-bit resolution at a sampling rate of 5 GHz over 40 μs the single-pixel signal and with 125 MHz over 2 ms the 320-pixel line.

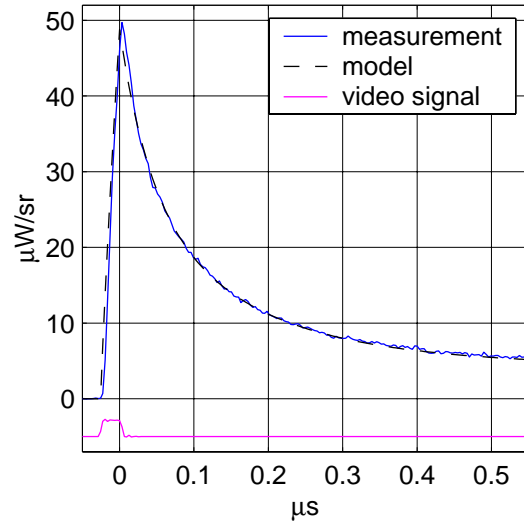
Averaging each signal over 256 frame repetitions reduced noise.

4.3. Results

Taking into account the solid angle covered by the photo sensor, its exact control voltage and resulting radiant sensitivity, as well as the input impedance of the oscilloscope, the recorded voltage can be converted into a radiant intensity (power per solid angle). The radiant sensitivity used is the one given in the sensor data sheet for 420 nm (blue) and can vary for up to a factor of two for other wavelengths. Because of this, and since no calibration source for radiant intensity was available, the resulting absolute values should only be seen as estimates. Figure 2 shows as an example the measured light output of the blue phosphor as well as the video input signal.

For further theoretical analysis as well as for optimizing the processing of signals for best readability, it is helpful to have a simple closed-form approximation of the phosphor impulse response. I manually adjusted the coefficients and number of terms in a sum of several exponential and power-law decay functions until the convolution of the resulting function with the video signal closely fitted the recorded photosensor output on a number of linear, logarithmic and double-logarithmic plots. This semi-manual fitting process

(a) Emission decay of a single pixel ($f_p = 36 \text{ MHz}$)



(b) Emission decay of a 320-pixel line

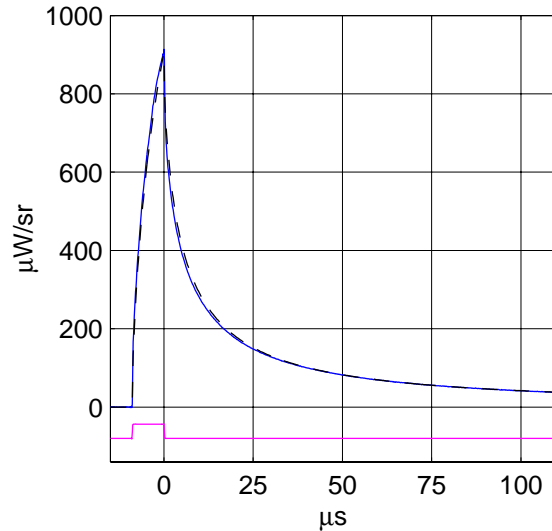


Figure 2. Blue phosphor decay measurement.

led to compacter and more accurately fitting impulse response functions than various parameter fitting algorithms that I tried.

I ended up with the following closed form approximation for the impulse response of the three phosphors:

$$P_{P22R}(t) / \frac{W}{V \cdot s \cdot sr} = 4 \times e^{-2\pi t \times 360 \text{ Hz}} + 1.75 \times e^{-2\pi t \times 1.6 \text{ kHz}} + 2 \times e^{-2\pi t \times 8 \text{ kHz}} + 2.25 \times e^{-2\pi t \times 25 \text{ kHz}} + 15 \times e^{-2\pi t \times 700 \text{ kHz}} + 29 \times e^{-2\pi t \times 7 \text{ MHz}} \quad (8)$$

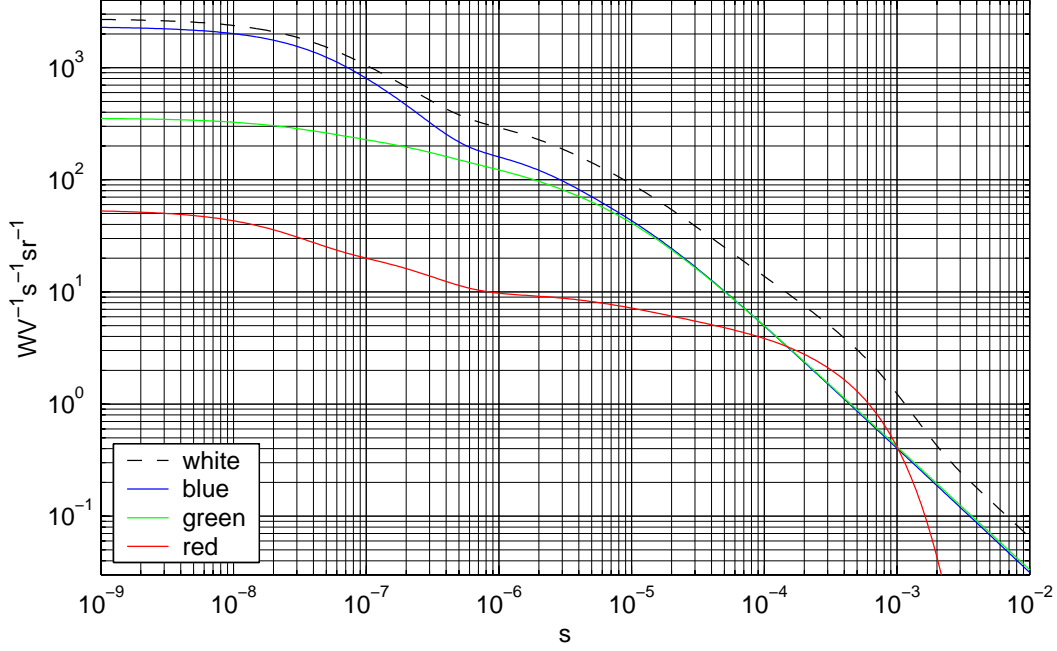


Figure 3. The numeric model of the measured P22 phosphor impulse response.

$$\begin{aligned}
 P_{P22G}(t) / \frac{W}{V \cdot s \cdot sr} = & \\
 & 210 \times 10^{-6} \times \left(\frac{t + 5.5 \mu s}{1 s} \right)^{-1.1} + \\
 & 37 \times e^{-2\pi t \times 150 \text{ kHz}} + \\
 & 100 \times e^{-2\pi t \times 700 \text{ kHz}} + 90 \times e^{-2\pi t \times 5 \text{ MHz}} \quad (9)
 \end{aligned}$$

$$\begin{aligned}
 P_{P22B}(t) / \frac{W}{V \cdot s \cdot sr} = & \\
 & 190 \times 10^{-6} \times \left(\frac{t + 5 \mu s}{1 s} \right)^{-1.11} + \\
 & 75 \times e^{-2\pi t \times 100 \text{ kHz}} + \\
 & 1000 \times e^{-2\pi t \times 1.1 \text{ MHz}} + \\
 & 1100 \times e^{-2\pi t \times 4 \text{ MHz}} \quad (10)
 \end{aligned}$$

$$P_{P22} = P_{P22R} + P_{P22G} + P_{P22B} \quad (11)$$

After convolution with the 1 V video signal according to (3) and a delay of 29 ns (transmission times in electron tubes and signal cables), these impulse response functions lead to the excellently matching dashed lines in Fig. 2.

All three phosphors show a very noticeable relative drop of radiant intensity in the first tenth of a microsecond. Figure 3 shows that of all three phosphors, the blue one has with $-1500 \text{ W}/(\text{V} \cdot \text{s} \cdot \text{sr})$ by far the largest drop in absolute intensity in the first 100 ns and therefore will provide the strongest high-frequency signal, while the red phosphor has

with $-34 \text{ W}/(\text{V} \cdot \text{s} \cdot \text{sr})$ the smallest absolute drop.

The Fourier transforms of the impulse response curves in Fig. 5 show that the blue phosphor applies to the video signal a low-pass filter in which for example a 10 MHz component is less than 40 dB more attenuated than a 1 kHz signal. Only for frequencies above around 5–10 MHz, the phosphors show the continuous 20 dB per decade roll-off typical for a first order low-pass filter.

Figure 4 shows as continuous lines the impulse response curves on a logarithmic time scale. Their amplitudes have been normalized to $P(0) = 1$ in this representation in order to make the curve forms more comparable. The dashed lines represent the integrals of the decay functions and show which fraction of the totally emitted energy after stimulation ceased has already been given off at any point in time.

The red phosphor, which decays purely exponentially, emits practically all of its stored energy within 1–2 ms, but it still has not lost a significant part of its energy within the first 10 μs . The blue and green phosphors show a far more heavy-tailed behavior, thanks to the power-law component in their impulse response. Even long after the stimulus, they still have not emitted all of their stored energy and as a result, even an unaided human observer with fully adapted scotopic vision can notice an afterglow on a CRT screen in an otherwise completely dark room for several minutes.

It might be worth noting that the integral of $P_{P22G}(t)$ shows even hours after the excitation some unreleased energy in this phosphor type. Although this measurement was not designed to estimate the here significant parameter β

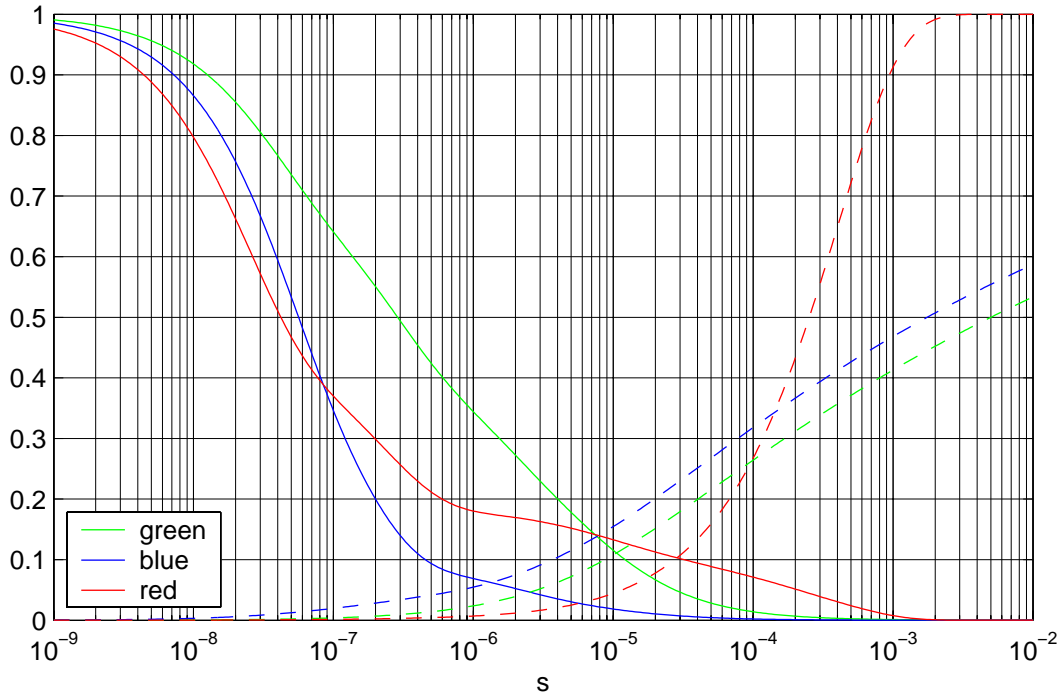


Figure 4. Normalized linear intensity impulse response curves and corresponding integrals (dashed).

in (6) with good accuracy, this observation still leads to the question whether CRT phosphors could leak confidential information not only via instantaneous compromising emanation, but also via data remanence.

5. Optical eavesdropping demonstration

Perhaps more interesting than a theoretical discussion of phosphor decay frequency characteristics is a visually convincing actual reconstruction of a displayed image from an out-of-sight CRT surface.

In the following experiment, the same monitor (Dell D1025HE) faces a white office wall at around a meter distance. The photomultiplier is now located behind the monitor, facing the same wall at around 1.5 m distance. There is no direct line of sight between the sensor and the screen surface.

As the wall illuminated by the monitor covers a large solid angle as seen from the photosensor, no additional optical elements such as a focusing lens are needed in this demonstration. The experiment was performed at night with the room lights switched off, however the room was far from completely dark, being illuminated by several computer displays and stray light from outside lamps.

Figure 6 shows a simple readability test chart with text in various sizes, which the monitor displayed as the tar-

get video signal during the test. This test image was displayed in the same video mode as before (VESA 640 × 480@85Hz). The text is in full white on black, and additional test letters show all full intensity combinations of the three phosphor colors. The oscilloscope averaged 256 frames (or equivalently 3 s of signal) at a sampling frequency of 250 MHz. (These exact parameters are not critical and quite acceptable readability of small text can also be achieved with lower sampling rates and numbers of averaged frames as well as higher video modes.)

Figure 7 shows the recorded and averaged photocurrent as a gray-scale image, much like a monitor driven with appropriate sync pulses would present it. The largest font sizes are readable, though the slow decay smears the luminosity of each white pixel along the path of the electron beam across the rest of the line and further. The gray values of all the rastered signals shown here were adjusted such that the values of the 0.1% highest and 0.1% lowest pixels in a histogram are all mapped to full white or full dark respectively, and the remaining values are linearly mapped to the corresponding points on a gray scale.

The raw photomultiplier current in Fig. 7 clearly has to be processed further in order to make text readable. Analog preprocessing has the advantage that it can improve significantly the signal-to-noise ratio before any amplification and quantization steps limit the dynamic range of the sig-

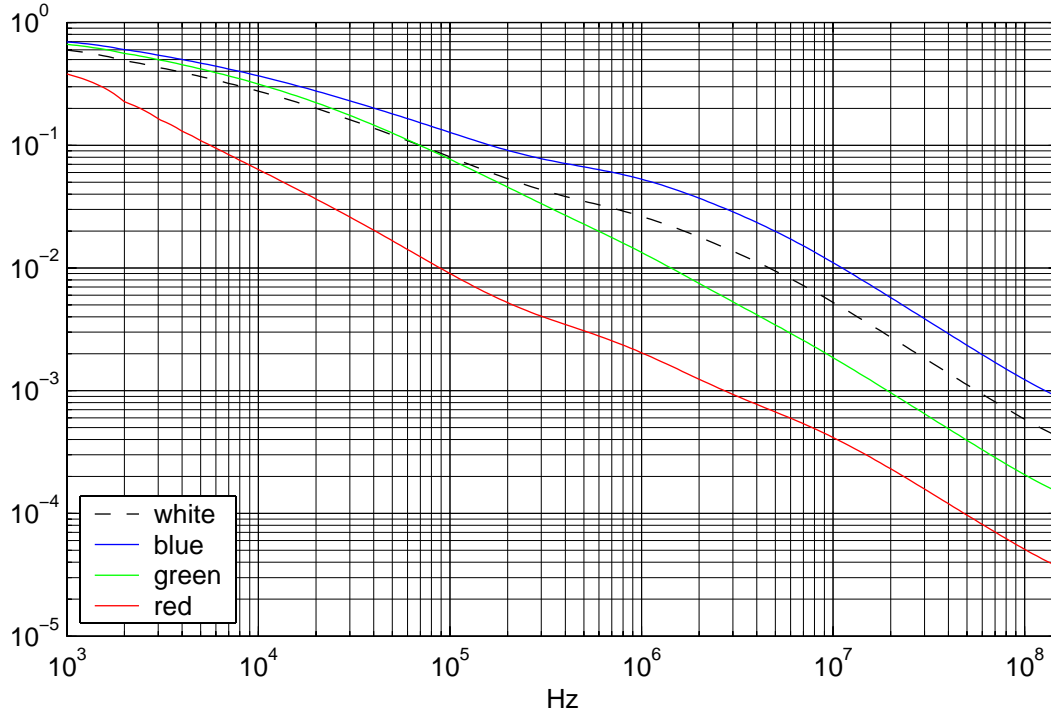


Figure 5. This figure shows the frequency characteristic of the three measured P22 phosphors and their combination to white. The modeled impulse response was truncated with a rectangular window to 3 ms and then a 512 kilosample FFT applied. The 0 Hz value has been normalized to equal 1 for all four curves.

nal to, for example, 8 bits in the case of the oscilloscope that was used. With a digitized signal of too low a quality, further digital recovery becomes difficult as the necessary high-pass filter step amplifies high-frequency noise further and a tradeoff has to be found between deconvolution and noise control.

Figure 8 shows the digital simulation of a simple first-order Butterworth high-pass filter with a cut-off frequency of 4 MHz applied to the signal. Such a filter could be implemented quite easily as just a resistor-capacitor combination. Its application leads to a dramatic improvement in text readability, though the resulting image still shows quite noticeable distortions. These are due to the fact that this simple filter applies a 20 dB per decade roll-off from 4 to 0 MHz, whereas the frequency characteristic of the phosphors (Fig 5) is actually significantly flatter below 4 MHz.

A much better reconstruction can be obtained by deconvolution, that is with the help of a filter that has approximately the inverse phase and frequency characteristic of the phosphor. To generate the image $\tilde{v}(t)$ in Fig. 9, I sampled the model impulse response function $P_{P22}(t)$ with the same sampling frequency and number of samples as the recorded averaged luminosity signal $I(t)$ for a single frame, then

Fourier transformed both, divided the complex results, and applied the inverse Fourier transform:

$$\tilde{v} = \mathcal{F}^{-1} \left\{ \frac{\mathcal{F}\{I\}}{\mathcal{F}\{P_{P22}\}} \right\} \quad (12)$$

No padding was necessary before performing the Fourier transform since $I(t)$ is a periodic signal anyway, $P_{P22}(t)$ has already dropped close to zero near the beginning of the frame period, and the FFTW code [17] used to perform the calculation can also handle block sizes other than 2^n for the discrete Fourier transform quite efficiently.

The result of the deconvolution shows a significantly improved contrast, the smear along the electron beam path to the right of each illuminated pixel is reduced, and even the smallest font size of the test chart (with an H-height of 8 pixels or 4 mm) becomes readable.

Slightly sharper edges can be restored for blue text than for green (and consequently white) text, which confirms what the measured frequency characteristic of the three phosphors in Fig. 5 already suggested. The high-frequency components of the red signal remain too weak for this sensor setup.

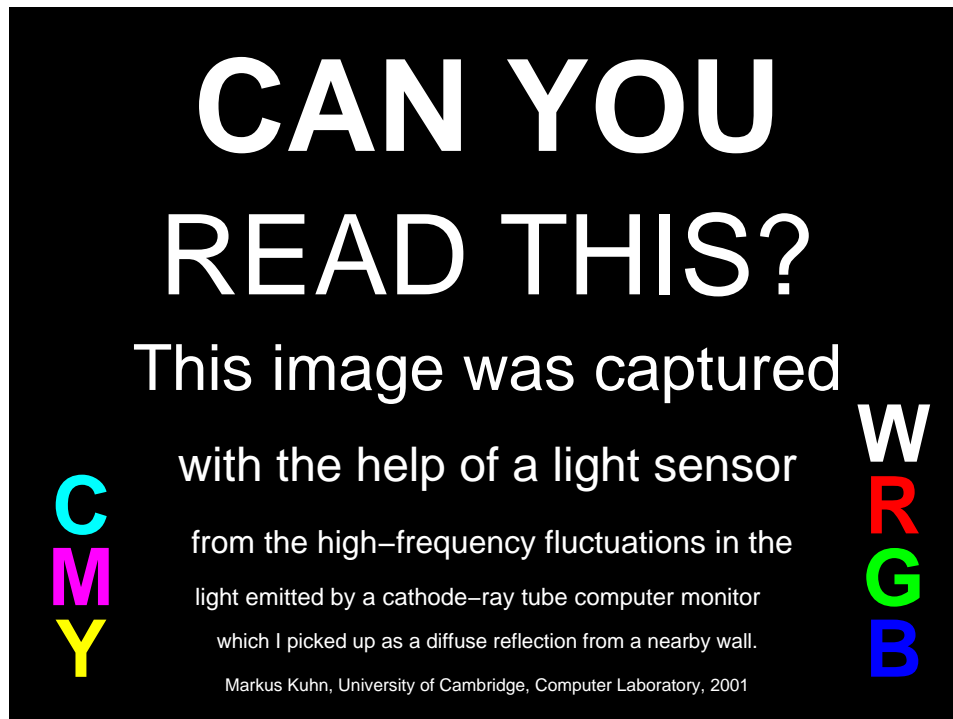


Figure 6. Testchart displayed on the target monitor in VESA 640x480@85Hz video mode.

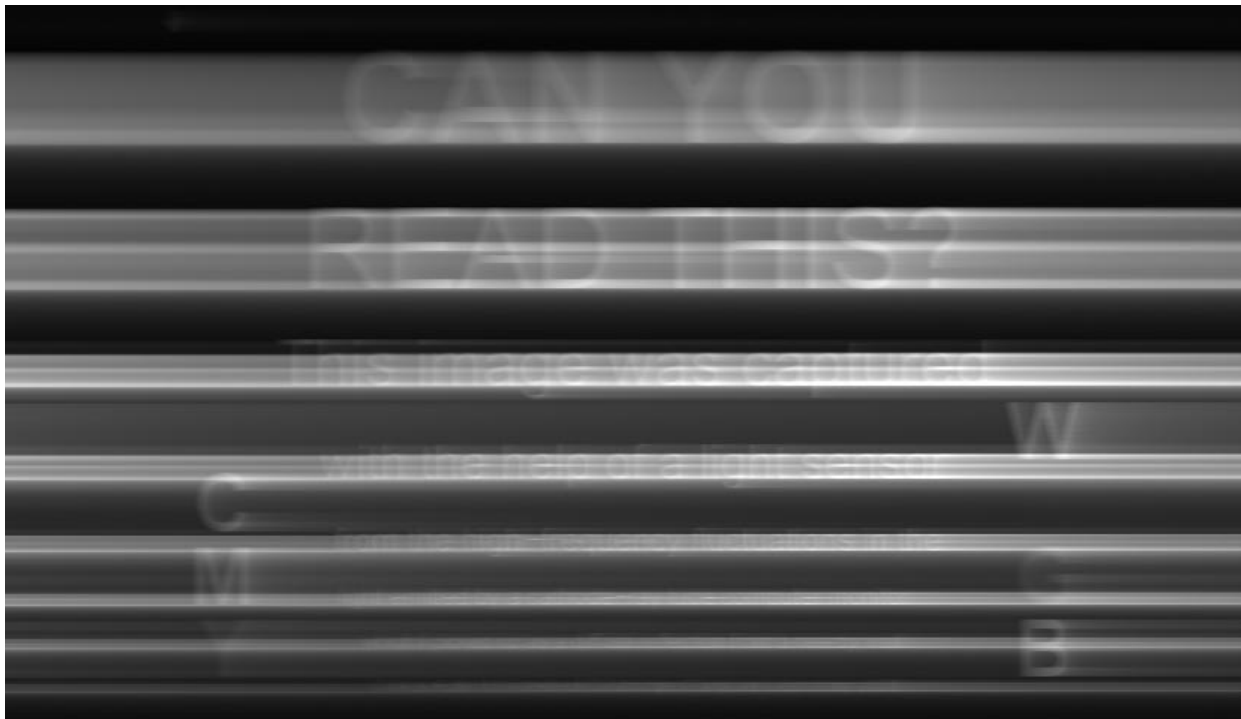


Figure 7. Unprocessed photomultiplier output signal after diffuse reflection from a wall.

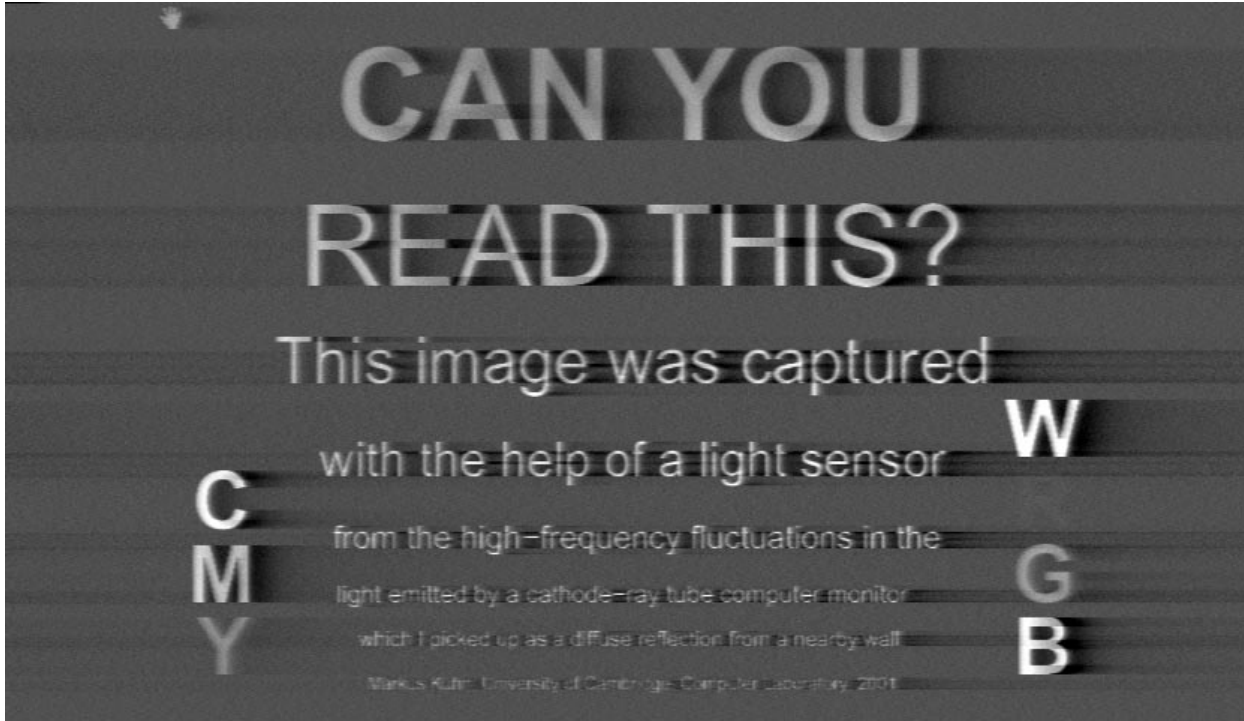


Figure 8. Signal from Fig. 7 after application of a 4 MHz Butterworth high-pass filter.

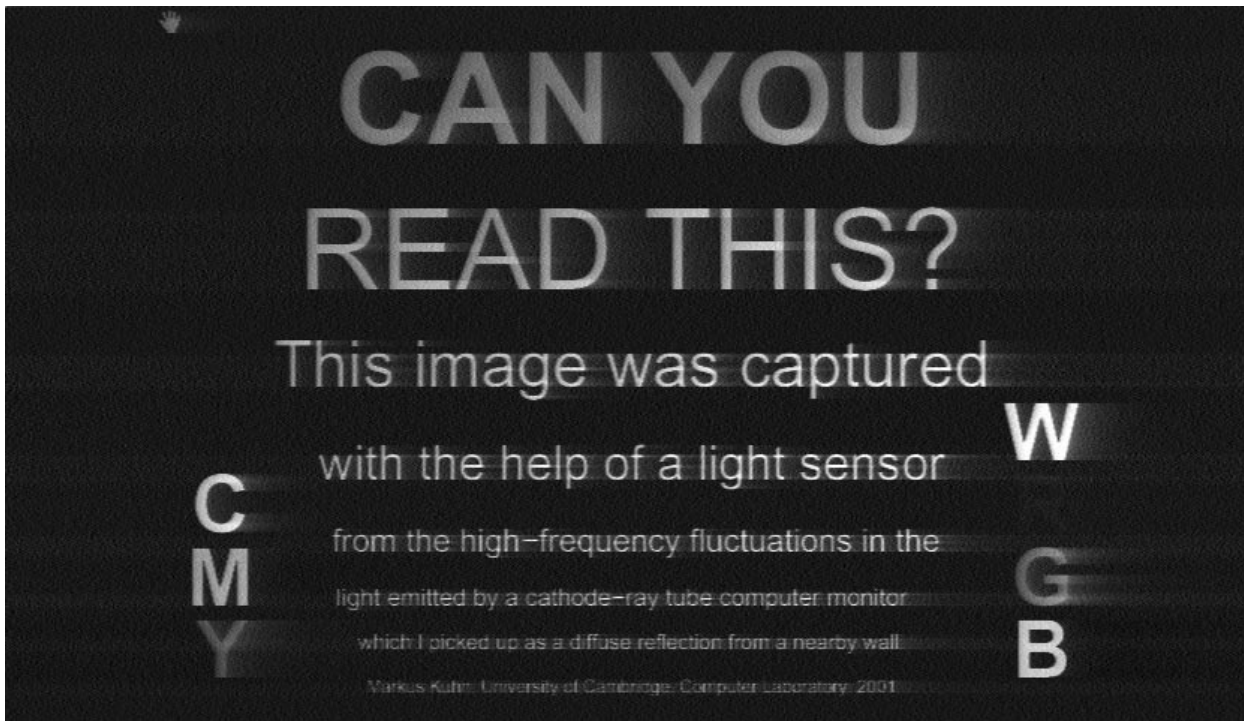


Figure 9. Signal from Fig. 7 after application of a matched deconvolution filter (inverse frequency characteristic to that of white shown in Fig. 5).

6. Threat analysis

With the help of a phosphor decay curve like the one shown in Fig. 3, we can now estimate the signal strength that an eavesdropper can receive and what upper bound on the reception distance is imposed by shot noise. For definitions of the radiometric and photometric quantities and SI units used here, see [16, 18].² For the following order-of-magnitude estimates, we assume in the interest of simplicity that the screen, wall, and sensor surfaces involved are roughly parallel to each other and that the photons of interest travel perpendicular to these, otherwise the cosine of the relevant angles would have to be multiplied in as well.

6.1. Direct observation

We first consider the case without diffuse reflection from a wall, where the eavesdropper can see the screen surface directly. This might allow projective observation with a telescope, but the result might not be satisfactory in situations with minor distortions such as aperture diffraction, atmospheric fluctuations or even a frosted glass window. Time-domain analysis of the received light could be of interest even where a line of sight is available.

Let $t_p = f_p^{-1}$ be the duration for which the electron beam illuminates a single pixel. The video voltage due to one pixel (full intensity: $V = 1$ V) will be

$$v_\gamma(t) = \begin{cases} V & \text{if } 0 < t \leq t_p \\ 0 & \text{otherwise} \end{cases} \quad (13)$$

and the resulting radiant intensity according to (3) is

$$I_p(t) = V \cdot \int_{t-t_p}^t P(t') dt'. \quad (14)$$

At distance d with receiver aperture area A_r , neglecting transmission delays and the directional characteristic of the emitter, the power received from the pixel is

$$P_p(t) = \frac{A_r}{d^2} \cdot I_p(t). \quad (15)$$

We approximate the detection process performed in the receiver by simply integrating the received pixel power over

²In a nutshell: Luminous flux is measured in lumen (lm), which is the photometric equivalent of radiation power, weighted by the spectral sensitivity of the human eye, where 683 lm are per definition as bright as 1 W of (green) 540 THz light. In order-of-magnitude calculations, I will simply approximate 10^3 lm as 1 W. The steradian (sr) measures a solid angle (4π for the full sphere), candela (cd) is the same as lumen per steradian and measures the luminous intensity of a light source in a given direction, and lux (lx) is the same as lumen per square meter and measures the illuminance of a location. Commonly encountered illuminance levels cover ten orders of magnitude, from 10^5 lx for "direct sunlight" to 10^{-4} lx for "overcast night sky (no moon or light pollution)" [16, p. 16].

the pixel duration. The resulting energy collected per pixel is

$$Q_p = n \cdot \int_0^{t_p} P_p(t) dt \quad (16)$$

where n is the number of frame repetitions accumulated by periodic averaging. This is only a small fraction of the overall energy received from the pixel during its decay, but it approximates roughly the amount of energy that can be separated from the contributions of neighbor pixels by high-pass filtering. At wavelength λ this energy corresponds to

$$N_p = \frac{Q_p \lambda}{hc} \quad (17)$$

photons per pixel ($hc = 1.986 \times 10^{-25}$ Jm).

We also have to consider background light as a noise source, both from other pixels of the observed CRT as well as any surrounding surfaces. The photon count per pixel duration from the background light can be estimated as

$$N_b = \frac{nt_p A A_r L_b \lambda}{hcd^2}, \quad (18)$$

where L_b is the average radiance and A is the area of the observed background surface.

The arrival of photons at a detector aperture is a Poisson process [19]. This means that when a random variable N describes the number of photons received per pixel and we expect $\mathcal{E}[N]$ photons on average then the standard deviation $\sqrt{\mathcal{E}[(N - \mathcal{E}[N])^2]}$ will be $\sqrt{\mathcal{E}[N]}$. This inevitable variability of the photon count is known as *shot noise*. As $N_b \gg N_p$, the background light determines the amount of shot noise against which the status of a single pixel has to be detected. This roughly becomes feasible when the signal-to-noise ratio is greater than one, that is

$$N_p > \sqrt{N_b} \quad (19)$$

or with $P(t) \approx P(0)$ for $0 \leq t \leq t_p$

$$\frac{nt_p^2 A_r V P(0) \lambda}{2hcd^2} > \sqrt{\frac{nt_p A A_r L_b \lambda}{hcd^2}}. \quad (20)$$

and therefore

$$\frac{A_r}{d^2} > \frac{4AhcL_b}{n\lambda V^2 t_p^3 P^2(0)}. \quad (21)$$

We can now fill this condition with some example parameters. Assuming a background luminance of 100 cd/m², as it is typical for a CRT and other bright surfaces in a well-lit office environment [16, 10], the corresponding background radiance will be in the order of not more than $L_b = 0.1$ W/(sr · m²), from which we mask off an observed area of $A = 0.2$ m². Together with other typical parameters such as $t_p = 20$ ns, $P(0) = 10^3$ W/(V · s · sr), $V = 1$ V, $\lambda = 500$ nm, and by averaging $n = 100$ frames, we get

$$\frac{A_r}{d^2} > 4 \times 10^{-5} \text{ sr}. \quad (22)$$

For example, a simple telescope with $A_r = 0.3 \text{ m}^2$ could therefore theoretically receive a signal under these well-lit conditions up to in the order of 80 m away.

6.2. Indirect observation

We now consider an indirect observation in a dark environment, where the not directly visible CRT screen faces at distance d' a diffusely reflecting observable wall, which has a reflection factor $0 < \rho < 1$. The radiant intensity (power per solid angle) $I_p(t)$ from a pixel will lead to an irradiance (incoming power per area)

$$E_p(t) = \frac{I_p(t)}{d'^2} \quad (23)$$

onto the wall and to a radiant exitance (outgoing power per area) of

$$M_p(t) = \rho E_p(t). \quad (24)$$

For a uniformly diffusing (“Lambertian”) surface, we have to divide the radiant exitance by π [16] to obtain the corresponding radiance (power per solid angle per area)

$$L_p(t) = \frac{1}{\pi} M_p(t) \quad (25)$$

which leads us finally to the power

$$P_p(t) = \frac{AA_r}{d^2} \cdot L_p(t) \quad (26)$$

passing through the receiver aperture A_r , which is located at distance d from the observed wall area A . Using the same $P(t) \approx P(0)$ for $0 \leq t \leq t_p$ approximation as before, we can estimate the number

$$N_p = \frac{\rho n t_p^2 A A_r V P(0) \lambda}{2\pi h c d^2 d'^2} \quad (27)$$

of photons received from a single pixel and compare it to the number

$$N_b = \frac{n t_p A A_r \rho E_b \lambda}{\pi h c d^2}, \quad (28)$$

of photons received from the background light, assuming the wall is exposed to an irradiance E_b . The signal to shot-noise ratio will again be of order unity under the condition $N_p > \sqrt{N_b}$, which leads to a receivability condition

$$\frac{A_r}{d^2} > \frac{4\pi E_b h c d'^4}{\rho n \lambda t_p^3 A V^2 P^2(0)}. \quad (29)$$

Let’s again look at an example scenario. Assuming the observed monitor has a luminous intensity of $100 \text{ cd/m}^2 \times 240 \text{ mm} \times 320 \text{ mm} = 8 \text{ cd}$, a wall at a distance $d' = 2 \text{ m}$ would be exposed to an illuminance of in the order of 2 lx from the overall light given of by the monitor alone, which

corresponds to the illuminance during “late twilight” [16] and is equivalent to an irradiance of in the order of $E_b = 1 \text{ mW/m}^2$. Using this with the same example parameters as before, as well as $A = 2 \text{ m}^2$ and $\rho = 0.5$, we get

$$\frac{A_r}{d^2} > 1 \times 10^{-4} \text{ sr} \quad (30)$$

for this indirect observation under late twilight conditions. The $A_r = 0.3 \text{ m}^2$ mirror used as an example before could therefore receive a signal under these conditions up to in the order of 50 m. This distance is proportional to $1/\sqrt{E_b}$, so for example under full daylight illuminance (10^4 lx), observation would already be infeasible just one meter from the wall.

6.3. Observation of other displays

It is worth noting that the very high pixel frequencies used by CRTs play a significant rôle in limiting the reception range. Optical displays with lower update frequencies could also pose an eavesdropping risk, even if they do not offer the redundancy of a repetitive video signal. A practical example would be devices with slow serial ports (10^4 – 10^5 bit/s), such as some modems, that feature light-emitting diodes (LEDs) to indicate optically the logic level of data lines. Unless the displayed signal is distorted, for example by a monostable-multivibrator circuit that enforces a minimum on period of at least a byte time, an optical eavesdropper could manage to reconstruct transmitted data by monitoring the LED luminosity at a distance.

Another example would be software-controllable status LEDs such as those connected to the keyboard and hard-disk controller of every PC, and also of course the infrared ports found in many mobile computers. Malicious software could use these in order to covertly broadcast information in situations where this cannot be accomplished via normal network connections (e.g., due to “air gap” security or a mandatory access-control operating system).

A link budget and shot noise calculation very similar to the one developed in the previous sections can be used here as well to estimate what upper bounds for bit error rates an eavesdropper has to expect depending on the distance and background illumination.

Normal LEDs have a luminous intensity of in the order of 1–10 mcd, although super-bright variants with up to 100 mcd or more are available as well. We can again estimate the expected number of photons N_p received from a single bit pulse of the LED, as well as the expected number N_b from the background illumination. For a sufficiently large N_b , we can approximate the distribution of the number N of photons received as a normal distribution

$$P\left(\frac{N - \mu}{\sigma} < x\right) \approx \frac{1}{\sqrt{2\pi}} \int_{-\infty}^x e^{-\frac{y^2}{2}} dy \quad (31)$$

with the mean value

$$\mu = \begin{cases} N_b + N_p & \text{when LED on} \\ N_b & \text{when LED off} \end{cases} \quad (32)$$

and the standard deviation

$$\sigma = \sqrt{N_b}. \quad (33)$$

Assuming that transmitted bits 0 and 1 are equally likely, a matched filter detector [20] will count the photons N received per bit interval and compare the resulting number with the threshold $N_b + \frac{1}{2}N_p$ to decide whether the LED was on or not. The probability for a bit error due to shot noise will therefore be

$$p_{\text{BER}} = Q\left(\frac{N_p}{2\sqrt{N_b}}\right) \quad (34)$$

where

$$\begin{aligned} Q(x) &= \frac{1}{\sqrt{2\pi}} \int_x^{\infty} e^{-\frac{y^2}{2}} dy \\ &= \frac{1}{2} - \frac{1}{2} \operatorname{erf}\left(\frac{x}{\sqrt{2}}\right) \approx \frac{e^{-\frac{x^2}{2}}}{x\sqrt{2\pi}} \quad (\text{if } x > 3) \end{aligned} \quad (35)$$

is the Gaussian error integral [20].

As a practical example, we consider a direct line of sight to a green ($\lambda = 565$ nm) LED with a luminous intensity of 7 mcd, which corresponds to a radiant intensity of roughly $I_p = 10^{-5}$ W/sr. A telescope at distance d with aperture A_r will receive over a single bit pulse time t_p an expected number of photons

$$N_p = \frac{t_p A_r I_p \lambda}{hcd^2} \quad (36)$$

from the LED plus an expected number of photons

$$N_b = \frac{t_p A A_r \rho E_b \lambda}{\pi hcd^2}, \quad (37)$$

if the observed area A has a reflection factor ρ and is exposed to an ambient irradiance E_b . With example parameters $A_r = 0.3$ m², $d = 500$ m, $t_p = 10^{-5}$ s (100 kbit/s), $\rho = 1$, $A = 1$ cm² = 10^{-4} m² and $E_b = 1$ W/m² (roughly 10^3 lx, “overcast sky”), we end up with a lower bound for the bit error rate of 10^{-7} .

Finally an example where the same LED illuminates a wall at distance d' , of which the eavesdropper observes area A and collects from a single bit pulse an expected photon count

$$N_p = \frac{t_p A A_r \rho I_p \lambda}{\pi hcd^2 d'^2}, \quad (38)$$

whereas the photon count from the background illumination remains as in (37). Inserting example values of $A_r = 0.3$ m², $d = 50$ m, $t_p = 10^{-4}$ s (10 kbit/s), $\rho = 0.5$,

$d' = 2$ m, $A = 2$ m² and $E_b = 1$ mW/m² (roughly 1 lx, “late twilight”), we end up with a lower bound for the bit error rate near 10^{-4} .

Figure 10 illustrates a possible detection and clock recovery algorithm for NRZ encoded binary data (as it appears on serial port lines), which recovers the sampling clock signal if only the bitrate is known (or guessed correctly).

7. Receiver design considerations

The experiment in Section 5 shows the image quality that an eavesdropper can achieve in principle under favorable conditions by using simple off-the-shelf instruments. It is just intended as a proof-of-concept laboratory demonstration for the diffuse optical CRT eavesdropping risk and does not exploit a number of techniques for improving range and signal quality that could be used in purpose-built portable optical eavesdropping receivers.

The most important improvement is the use of a zoom telescope to capture more photons and provide for the exact selection of a target area with good signal-to-noise ratio. The image quality of the telescope needs to be only good enough to allow for the masking of an area of interest, usually with centimeter to decimeter resolution. This avoids the need for high-precision mirrors such as those used for astronomic imaging and should simplify the construction of receivers with large apertures.

The ultimate performance limit is the amount of background light and the associated shot noise that reaches the photosensor. An important design concern will be techniques for suppressing light from unwanted sources. This can be achieved with the help of careful geometric masking, time-domain masking, and wavelength filtering.

The data provided for “X” and “XX” screen phosphors in [13] shows that the zinc-sulfide based blue and green phosphors have a bell-shaped spectral energy distribution centered mostly at 450 and 520 nm, respectively, with a standard deviation of roughly 20–30 nm. The red phosphors on the other hand typically have a spectrum consisting of several much narrower lines, usually near 630, 620 and 600 nm with a standard deviation of less than 5 nm. Color filters or a spectrometer can be used to separate the contributions from different phosphors to reconstruct color images or apply phosphor-specific deconvolution parameters. Careful selection of filter frequencies can also be used to attenuate background light. While both the sun and incandescent lights have a relatively flat spectrum in the optical band, this is not the case with some types of fluorescent lights commonly used in offices, which emit much of their energy in a few narrow spectral lines that could be suppressed with suitable filters.

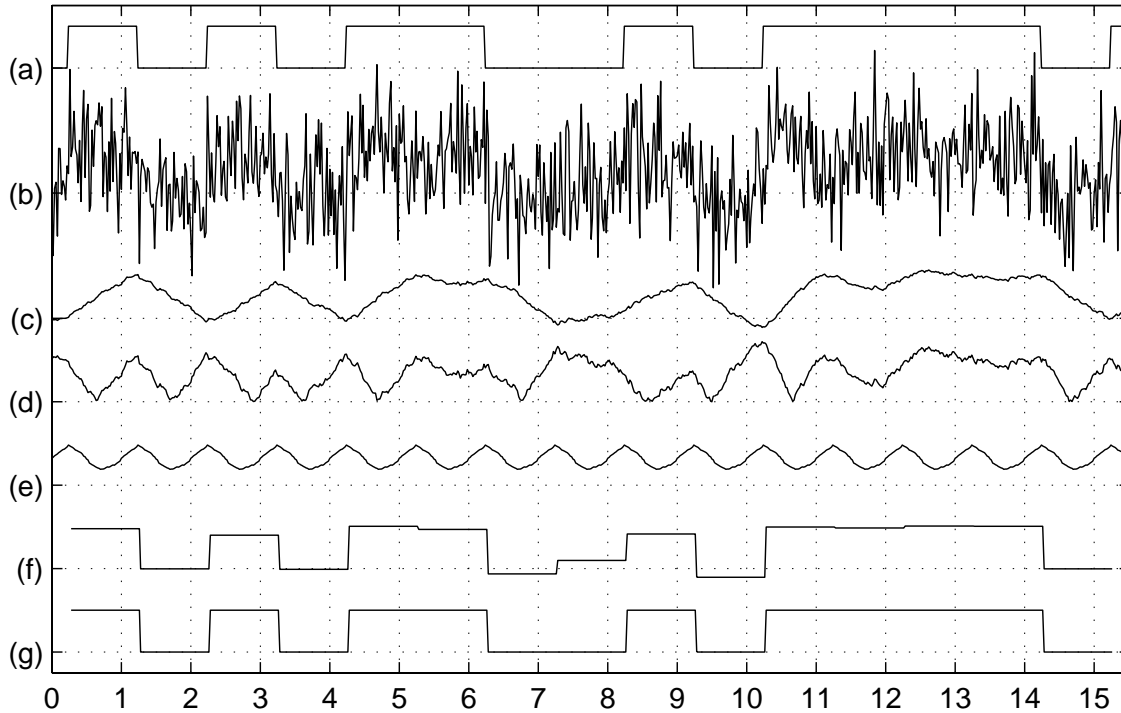


Figure 10. This chart illustrates an algorithm for clock and data signal recovery from a NRZ binary signal (a) with added white Gaussian noise (b). We first convolve the received signal (b) with the pulse shape of a single bit (here a rectangular pulse) and obtain (c). Curve (d) shows the distance of (c) from its mean, which we convolve with an impulse series with the same period as the bit length to get (e). The result has maxima at the edges of the original signal, which provides us with the clock signal for sampling (c). The sampled values (f) are then thresholded (g) and we have recovered the original bitstream (a) out of (b) knowing only its bit rate but not its clock phase.

The phosphor decay curves shown in this paper were measured with a sensor that is sensitive over the entire optical band. It might be worth investigating, whether narrow-band sensors observe different decay curves for different spectral lines. If this is the case, spectral bands with particularly low high-frequency attenuation could be selected by an optical eavesdropping receiver to improve the signal quality further, although a tradeoff will have to be made between optical bandwidth and shot noise.

If background light is generated directly from a 50 or 60 Hz power supply, it will be modulated with twice that frequency; fluorescent lights far more so than incandescent ones. Where the observed signal is repetitive, varying the receiver gain inversely proportional to the background light amplitude can further improve the signal-to-noise ratio.

Analog preprocessing at the output of the photosensor could better approximate the optimal deconvolution filter than just the resistor-capacitor combination simulated in the previous section. Digital processing would then have to take care only of any remaining inaccuracies of the analog stage.

8. Countermeasures

Once the nature of a new eavesdropping technique is understood, it is possible to suggest a range of countermeasures that when combined and implemented properly can significantly reduce the described risk.

Display surfaces as well as keyboards used for handling critical information should naturally be kept out of any line of sight to a potential eavesdropper. In addition, also diffusely reflected stray light from cathode-ray tube displays should be treated as a potentially compromising emanation, especially when there is low background illumination and eavesdroppers can install large-aperture equipment within a few hundred meters. Rooms where a significant amount of the ambient light comes from displayed sensitive information should be shielded appropriately, for example by avoiding windows.

Various measures for jamming diffuse optical emissions with good background illumination can be used. Background light should preferably be of a broadband nature

(solar or incandescent) or in the case of fluorescent lights be produced with phosphors that have an emission spectrum similar to that of CRT phosphors. Modern fluorescent lights that are operated with a high-frequency current (≥ 20 kHz) are preferable as they have significantly reduced dark phases and in addition individual lamps will not be phase synchronized.

Some types of monitors include already an ambient light sensor to adjust brightness and contrast automatically to the surrounding illumination. It would be easy to extend this mechanism such that a power-saving mode is activated when the ambient light levels fall below a secure jamming margin. Such a mechanism has not only security but also ecologic and ergonomic advantages. Less electric power would be wasted in dark and empty offices overnight if darkness acted as an additional power-saving mode trigger and eye strain for users might be prevented by discouraging work under bad background illumination.

The red phosphor in this demonstration showed a significantly better high-frequency attenuation than the green and blue phosphors. In order to facilitate the selection of suitable CRT phosphors for information security applications, it would be helpful if display tube and phosphor manufacturers as well as phosphor-type registries provided impulse-response information in the form of double-logarithmic diagrams such as Fig. 3 that cover a time scale of 10^{-9} – 10^{-2} s and perhaps even a closed-form approximation along with a plot of the frequency-domain filter characteristic. An example for a suitable characteristic parameter of interest in the design of a security CRT might be the relative attenuation provided by a phosphor for beam currents with 100 Hz and 10 MHz frequency. It would also be helpful if monitor manufacturers documented, which exact CRT and phosphor types as well as which beam currents they use.

The need for special security CRTs is likely to be reduced significantly with the further proliferation of liquid crystal displays (LCDs). Their pixels react considerably slower than CRT phosphors and most types of flat-panel displays refresh all pixels in a line simultaneously. Both these factors suggest that this technology has a significantly reduced risk of leaking information about individual pixels in diffuse optical emanations.

9. Conclusions

The information displayed on a modern cathode-ray tube computer monitor can be reconstructed by an eavesdropper from its distorted or even diffusely reflected light using easily available components such as a photomultiplier tube and a computer with suitably fast analog-to-digital converter.

Due to shot-noise limits, the eavesdropping from diffuse reflections of display light (both CRT and LED) seems only

applicable in relatively dark environments (e.g., “late twilight” or 1 lx) and is even then limited to less than a few tens or hundreds of meters distance, but that alone might already be of practical concern in some situations. Better eavesdropping distances even under office-light conditions become possible with a direct line of sight, which might include minor distortions such as frosted glass that would otherwise be deemed sufficient to frustrate projective observation.

Very much like radio-frequency eavesdropping of video displays, the practical exploitation of compromising optical time-domain emanations eavesdropping will usually require specially designed equipment, expertise, and patience. However it seems at least as powerful as the former, and organizations who have traditionally worried about compromising radio emanations should seriously consider this new set of eavesdropping techniques in their threat models.

10. Acknowledgment

The author has been supported by a European Commission Marie Curie training grant and would like to thank David Wheeler and Ross Anderson for their suggestions and encouragement, as well as the TAMPER Lab sponsors for making equipment purchases possible.

References

- [1] Deborah Russell, G. T. Gangemi Sr.: *Computer Security Basics*, Chapter 10: TEMPEST, O’Reilly & Associates, 1991.
- [2] NACSIM 5000: *Tempest Fundamentals*, National Security Agency, Fort George G. Meade, Maryland, February 1982. Partially declassified transcript: <http://cryptome.org/nacsim-5000.htm>
- [3] National Security Telecommunications and Information Systems Security Advisory Memorandum NSTISSAM TEMPEST/1-92: *Compromising Emanations Laboratory Test Requirements, Electromagnetics*, National Security Agency, Fort George G. Meade, Maryland, 15 December 1992. Partially declassified transcript: <http://cryptome.org/nsa-tempest.htm>
- [4] Wim van Eck: “Electromagnetic Radiation from Video Display Units: An Eavesdropping Risk?”, *Computers & Security*, Vol. 4, pp. 269–286, 1985.
- [5] Peter Smulders: “The Threat of Information Theft by Reception of Electromagnetic Radiation from RS-232 Cables”. *Computers & Security*, Vol. 9, 1990, pp. 53–58.

- [6] Erhard Möller, Lutz Bernstein, Ferdinand Kolberg: *Schutzmaßnahmen gegen kompromittierende elektromagnetische Emissionen von Bildschirmsichtgeräten [Protective Measures Against Compromising Electro Magnetic Radiation Emitted by Video Display Terminals]*, Labor für Nachrichtentechnik, Fachhochschule Aachen, Aachen, Germany
- [7] Markus G. Kuhn, Ross J. Anderson: “Soft Tempest: Hidden Data Transmission Using Electromagnetic Emanations”, in David Aucsmith (Ed.): *Information Hiding*, Second International Workshop, IH’98, Portland, Oregon, USA, April 15–17, 1998, Proceedings, LNCS 1525, Springer-Verlag, pp. 124–142.
- [8] Henri Hodara: “Secure Fiberoptic Communications”, *Symposium on Electromagnetic Security for Information Protection*, SEPI’91, Proceedings, Rome, Italy, 21–22 November 1991, Fondazione Ugo Bordoni, pp. 259–293.
- [9] *Monitor Timing Specifications*, Version 1.0, Revision 0.8, Video Electronics Standards Association (VESA), San Jose, California, September 17, 1998.
- [10] *Dell D1025HE Color Monitor User’s Guide*, ZF5368, April 1997.
- [11] *Measurement of Phosphor Persistence of CRT Screens*, Electronic Industries Alliance (EIA), Tube Electron Panel Advisory Council (TEPAC), Publication TEP105-14, Arlington, Virginia, April 1987.
- [12] *Worldwide Type Designation System for TV Picture Tubes and Monitor Tubes*, Electronic Industries Alliance (EIA), Tube Electron Panel Advisory Council (TEPAC), Publication TEP106-B, Arlington, Virginia, June 1988.
- [13] *Optical Characteristics of Cathode-Ray Tube Screens*, Electronic Industries Alliance (EIA), Tube Electron Panel Advisory Council (TEPAC), Publication TEP116-C, Arlington, Virginia, February 1993.
- [14] W. Wolf, H. Deubel: “P31 phosphor persistence at photopic mean luminance level”, *Spatial Vision*, Vol. 10, No. 4, 1997, pp. 323–333.
- [15] *Photosensor Modules H5773/H5783/H6779/H6780/H5784 Series*, Hamamatsu Photonics K.K., 2000. <http://www.hamamatsu.com/>
- [16] Peter A. Keller: *Electronic Display Measurement – Concepts, Techniques and Instrumentation*. John Wiley & Sons, New York, 1997.
- [17] Matteo Frigo, Steven G. Johnson: “FFTW: An Adaptive Software Architecture for the FFT”, *Proceedings of the International Conference on Acoustics, Speech, and Signal Processing*, Vol. 3, pp. 1381–1384, 1998. <http://www.fftw.org/>
- [18] *Quantities and units — Part 6: Light and related electromagnetic radiations*, International Standard ISO 31-6, International Organization for Standardization, Geneva, 1992.
- [19] Tudor E. Jenkins: *Optical Sensing Techniques and Signal Processing*, Prentice-Hall International, 1987.
- [20] Rodger E. Ziemer, Roger L. Peterson: *Digital Communications and Spread Spectrum Systems*, Macmillan, New York, 1985.